


# Simultaneous Determination of Thermal Conductivity and Heat Capacity in Thin Films with Picosecond Transient Thermoreflectance and Picosecond Laser Flash

Zefang Ye, Janghan Park, Yanyao Zhang, Xianghai Meng, Matthew Disiena, Sanjay K. Banerjee, Jung-Fu Lin & Yaguo Wang


To cite this article: Zefang Ye, Janghan Park, Yanyao Zhang, Xianghai Meng, Matthew Disiena, Sanjay K. Banerjee, Jung-Fu Lin & Yaguo Wang (2023) Simultaneous Determination of Thermal Conductivity and Heat Capacity in Thin Films with Picosecond Transient Thermoreflectance and Picosecond Laser Flash, *Nanoscale and Microscale Thermophysical Engineering*, 27:3-4, 182-194, DOI: [10.1080/15567265.2023.2255243](https://doi.org/10.1080/15567265.2023.2255243)

To link to this article: <https://doi.org/10.1080/15567265.2023.2255243>

 View supplementary material [↗](#)

 Published online: 12 Sep 2023.

 Submit your article to this journal [↗](#)

 Article views: 162

 View related articles [↗](#)

 View Crossmark data [↗](#)



# Simultaneous Determination of Thermal Conductivity and Heat Capacity in Thin Films with Picosecond Transient Thermoreflectance and Picosecond Laser Flash

Zefang Ye<sup>a</sup>, Janghan Park<sup>ID</sup><sup>a</sup>, Yanyao Zhang<sup>ID</sup><sup>b,c</sup>, Xianghai Meng<sup>a</sup>, Matthew Disiena<sup>ID</sup><sup>d</sup>, Sanjay K. Banerjee<sup>ID</sup><sup>d</sup>, Jung-Fu Lin<sup>ID</sup><sup>b,e</sup>, and Yaguo Wang<sup>ID</sup><sup>a,e</sup>

<sup>a</sup>Department of Mechanical Engineering, The University of Texas at Austin, Austin, Texas, USA; <sup>b</sup>Department of Earth and Planetary Sciences, Jackson School of Geosciences, The University of Texas at Austin, Austin, Texas, USA; <sup>c</sup>Earth and Planetary Sciences, Stanford University, Stanford, California, USA; <sup>d</sup>Microelectronic Research Center, Department of Electrical and Computer Engineering, The University of Texas at Austin, Austin, Texas, USA; <sup>e</sup>Texas Materials Institute, The University of Texas at Austin, Austin, Texas, USA

## ABSTRACT

Combining the picosecond transient thermoreflectance (ps-TTR) and picosecond laser flash (ps-LF) techniques, we have developed a novel method to simultaneously measure the thermal effusivity and the thermal diffusivity of metal thin films and determine the thermal conductivity ( $\kappa$ ) and the heat capacity ( $c_v$ ) altogether. In order to validate our approach and evaluate the uncertainties, we analyzed five different metal films (Al, Cr, Ni, Pt, and Ti) with thicknesses ranging from 297 nm to 1.2  $\mu\text{m}$ . Our results on thermal transport properties and heat capacity are consistent with reference values, with the uncertainties for the thermal conductivity and the heat capacity measurements below 25% and 15%, respectively. Compared with the ps-TTR technique alone, the combined approach substantially lowers the uncertainty of the thermal conductivity measurement. Uncertainty analyses on various materials show that this combined approach is capable of measuring most of the materials with a wide range of thicknesses, including those with low thermal conductivity (e.g., mica) down to thicknesses as small as 60 nm and ultrahigh thermal conductivity materials (such as cubic BAs) down to 1400 nm. Simultaneous measurement of thermal conductivity and heat capacity enables exploration of the thermal physical behavior of materials under various thermodynamic and mechanical perturbations, with potential applications in thermal management materials, solid-state phase transitions, and beyond.

## ARTICLE HISTORY


Received 30 March 2023  
Accepted 31 August 2023

## KEYWORDS

Picosecond transient thermoreflectance; picosecond laser flash; thermal conductivity; heat capacity

In-situ thermal properties characterization is critical for a broad range of scientific fields, including but not limited to thermal management, phase transition in solid-state physics, etc. Accurate determination of both  $c_v$  and  $\kappa$  during a phase transition is crucial for estimating the thermoelectric figure-of-merit and ensuring proper thermal management. In general, high thermal conductivity materials are more efficient at transferring heat away from the heat generation area, thus help avoid overheating and improve overall performance and reliability, while high heat capacity helps stabilize the device's temperature. Thus, adding a layer of material with both high heat conductivity and high heat storage ability would further benefit thermal management.

**CONTACT** Yaguo Wang  [yaguo.wang@austin.utexas.edu](mailto:yaguo.wang@austin.utexas.edu)  Department of Mechanical Engineering, The University of Texas at Austin, 204 E. Dean Keeton Street, Austin, Texas 78712, USA; Jung-Fu Lin  [afu@jsj.utexas.edu](mailto:afu@jsj.utexas.edu)  Department of Earth and Planetary Sciences, Jackson School of Geosciences, The University of Texas at Austin, 2305 Speedway Stop C1160, Austin, Texas 78712, USA

 Supplemental data for this article can be accessed online at <https://doi.org/10.1080/15567265.2023.2255243>

In solid-state physics,  $c_v$ , the second-order derivative of the thermodynamic Gibbs free energy, provides information about the nature of phase transition, including the type of phase transition and the critical point. For instance,  $c_v$  displays singularity at the critical point for the first-order phase transition, which reflects the latent heat – the absorption of energy without any temperature change [1–3]. While in certain types of second-order phase transition, such as paramagnetic to ferromagnetic transition and superconducting transition,  $c_v$  experiences an anomaly near the critical point [4–7]. Simultaneous determination of  $c_v$  and  $\kappa$  can reveal the charge carrier and lattice vibration behaviors near the phase transition.

Even though thermal conductivity and heat capacity are the two of the most common and important thermal properties for materials, in reality, most optical thermoreflectance-based measurements measure thermal diffusivity ( $\alpha = \kappa/c_v$ ) or effusivity ( $\varepsilon = \sqrt{c_v\kappa}$ ) and convert them to thermal conductivity (or heat capacity) with literature heat capacity (or thermal conductivity) data [8, 9]. Thermal diffusivity is related to the heat propagation rate inside the material, while thermal effusivity reflects how heat is exchanged between the sample and its surrounding materials. Whether  $\alpha$  or  $\varepsilon$  is measured depends on specific techniques. A traditional laser flash method uses a strong continuous wave (CW) light source to shine on one side of the sample, and an IR thermometer or a thermal couple to monitor the temperature increase on the other side [9, 10], which mainly reflects how fast the heat can propagate inside the sample. Hence the diffusivity is obtained. For the bulk material, the thermal diffusivity is easily calculated with the time to the temperature half maximum  $t_{\frac{1}{2}}$  and the sample thickness  $d$  through  $\alpha = 0.1388 \frac{d^2}{t_{\frac{1}{2}}}$  [9]. For thin films, Taketoshi et al. developed the ultrafast laser flash measurement using the picosecond and nanosecond laser as the heating source, and the temperature increase on the other side was recorded [11–14]. From the temperature arising profile, thermal diffusivity can be extracted either using analytical or numerical methods [9, 15–17]. With transient thermoreflectance (TTR) [18–20], where usually both the heating pulse (pump) and detecting light (probe, CW) are on the same side and the probe sits at the center of pump spot, thermal effusivity is measured because the probed signal reveals how fast the heat escapes from the heated location to the surrounding. For time-domain thermoreflectance (TDTR) [8, 21] and frequency-domain thermoreflectance (FDTR) [22, 23], what is measured depends on the heat penetration depth ( $d_{th}$ ) with respect to the thickness of the target layer ( $d$ ), and  $d_{th}$  is controlled by modulation frequency. When  $d_{th}$  is much smaller than  $d$ , the sample layer can be treated as semi-infinite, and the measured signal is sensitive to effusivity. When  $d_{th}$  is much larger than  $d$ , the signal is mainly sensitive to thermal conductivity [24, 25].

Note that heat capacity can be determined separately with differential scanning calorimetry/thermogravimetric analysis (DSC/TGA) method [26, 27], but the powder form of samples is usually required. Although there are devices developed for measuring heat capacity in thin films, their fabrication can be quite complex, making them unsuitable for use with many materials. For low-dimensional materials, usually, the heat capacity of bulk counterparts is used, and its validity is still questionable. In extreme environments, such as high-temperature or high-pressure cases, both the heat capacities and the thermal conductivities of most materials are not available. Although some frequency-dependent TDTR and FDTR can also measure the thermal conductivity and heat capacity together [22, 24], the FDTR is not a suitable technique when thermal diffusivity is lower than  $3 \times 10^{-6} \text{m}^2/\text{s}$  [22]. With TDTR, the signal is less sensitive to thermal conductivity when the thickness is smaller than the shortest thermal penetration depth, which is constrained by the maximum modulation frequency [28].

In this work, we combine the ps-TTR [20] and ps-LF [11, 12] techniques to measure thermal effusivity and diffusivity simultaneously and conduct global fitting to obtain both thermal conductivity and heat capacity. Five metal films with thicknesses ranging from 297 nm to 1.2  $\mu\text{m}$  are measured, with  $\kappa$  and  $c_v$  values consistent with reference data and uncertainties below 25% and 15%, respectively. This combined approach offers unique advantages on characterizing thermal properties, especially under extreme conditions, such as in a high-pressure diamond anvil cell (DAC).

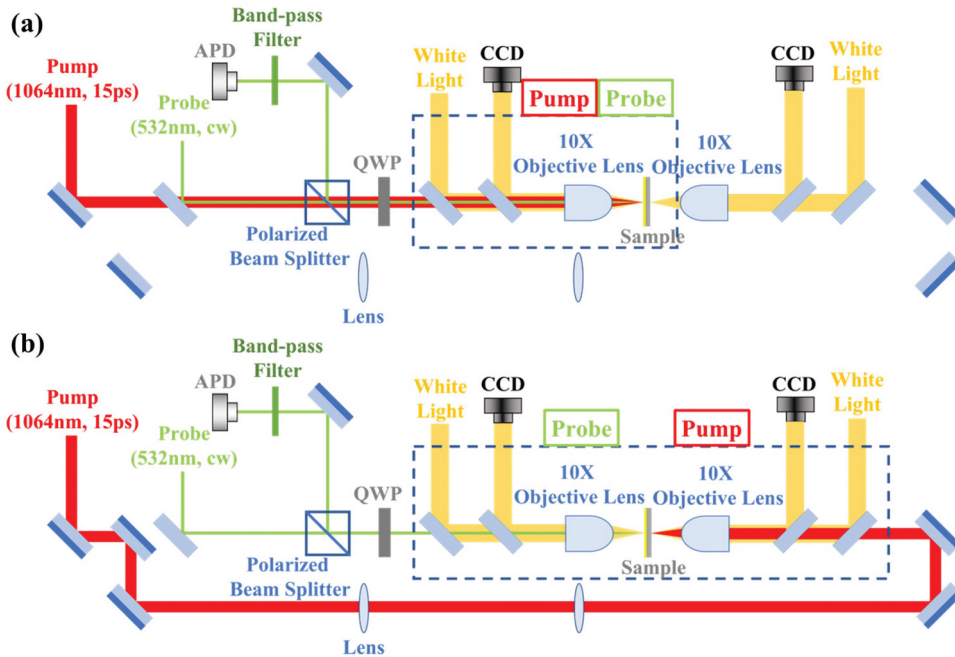


**Figure 1.** Optical layouts of the ps-TTR (a) and ps-LF systems (b). A flip mirror is used to switch the optical path of the pump laser (1064 nm, red lines) between the two systems.

The thermal effusivity is obtained with ps-TTR (Figure 1a) where the pump laser has 15 ps pulse duration (full width at half maximum) (Coherent Talisker Ultra 532–8, 1064 nm, 200 kHz repetition rate (1 kHz after passing through an acoustic-optical modulator (AOM)), 1 mW (pulse energy 1  $\mu$ J)) and probe is a CW laser (Coherent Verdi V6, 532 nm, CW, 1 mW). The pump and probe lasers are positioned on the same side of the sample, with the probe laser spot located at the center of the pump laser spot at the sample surface. A gold transducer layer coated at the probe side of the sample is used to increase the  $dR/dT$  ratio ( $\bar{2} \times 10^{-4} \text{K}^{-1}$ ) and to ensure low absorbance ( $<0.3$ ) at the probe wavelength (532 nm) [29]. The reflected probe is collected with a silicon avalanche photodiode (Hamamatsu C5658) with a time resolution of 500 ps and then recorded with an oscilloscope (Tektronics TDS 744A). With the gold transducer, the normalized reflectance change can be converted to the corresponding normalized temperature change at the gold surface (Refer to section S1 in the supplementary material). Since the separation time between pump pulses is 5 microseconds, it is possible to record a comprehensive thermal profile, spanning from the initial temperature to the peak and then to relaxation, without any thermal accumulation effect. The same ps-TTR setup is modified to perform ps-LF measurement (Figure 1b). The probe laser path remains the same as that of ps-TTR, while the pump laser is routed to heat the sample from the other side. A flip mirror is used to switch the pump beam path for the two measurement geometries. To differentiate the experimental setups, we will continue to name the front-pump front-probe configuration as ps-TTR and the back-pump front probe as ps-LF.

Five metal samples are measured with this combined approach. Four thin metal films (297 nm Nickel, 325 nm Chromium, 500 nm Aluminum, and 1107 nm Titanium) are deposited onto a 160  $\mu\text{m}$ -thick glass substrate using e-beam evaporation (Kurt J. Lesker, PVD75) or thermal evaporation (Kurt J. Lesker, NANO36). A 1.2  $\mu\text{m}$  Platinum foil is compressed from the Platinum powders (Goodfellow, 99.95% purity) in a high-pressure diamond anvil cell and then placed on the glass substrate. The films and foil thicknesses are determined with a profilometer (Dektak 6 M Stylus). All the samples are coated with a 60 nm gold layer as the thermal transducer using thermal evaporation.

We record the reflectance change at the surface of the gold layer separately using ps-TTR and ps-LF for each sample, resulting in two distinct experimental curves for every sample. A multi-layer 1D thermal diffusion model is then applied to fit and extract the thermal conductivity and heat capacity of the metal film.

The 1D assumption is made based on two factors. First, the diameter of the probe ( $10\ \mu\text{m}$ ,  $1/e^2$ ) is 10 times smaller than that of the pump ( $120\ \mu\text{m}$ ,  $1/e^2$ ), and the probe is located at the center of the pump. Due to the relatively flat temperature profile at the center of the Gaussian shape, we can assume the probed area has a relatively uniform heating profile and no temperature gradient along the radial direction. Second, the thermal penetration depth ( $d_{th} = \sqrt{\alpha t}$ ) is much shorter than the spot size of the pump. For ps-TTR, we examine the heat propagation within 100 ns, which is our fitting time. Aluminum is chosen to estimate  $d_{th}$  because of its highest thermal diffusivity ( $\alpha_{Al} = 9.7 \times 10^{-5}\text{m}^2/\text{s}$ ) among our measured samples, which is about  $3.1\ \mu\text{m}$  and significantly exceeds the 500 nm Al film thickness. Consequently, the heat propagates to the glass substrate within the first 100 ns. For the ps-LF, the metal film thickness, less than  $1.2\ \mu\text{m}$  for all five samples, serves as appropriated  $d_{th}$ . Since  $d_{th}$  remains much shorter than the pump's spot size in both cases, employing the 1D heat diffusion model is reasonable for both ps-TTR and ps-LF.

Given that all samples have the Au/Metal/Glass layered structure (Figure 2), we use the three-layer 1D thermal diffusion model solved with the Finite Difference Method to simulate both configurations, as described with Equation (1–4)[19, 30, 31].

$$\rho_1 c_1 \left( \frac{\partial T_1}{\partial t} \right) = \frac{\partial}{\partial z} \left( \kappa_1 \frac{\partial T_1}{\partial z} \right) + Source(z, t) \quad (1)$$

$$Source(z, t) = \frac{0.94(1 - R_{pump})F}{t_p \delta \left[ 1 - \exp\left(-\frac{z}{\delta}\right) \right]} \exp \left[ -2.77 \frac{(t - 2t_p)^2}{t_p^2} - \frac{z}{\delta} \right] \quad (2)$$

$$\rho_i c_i \left( \frac{\partial T_i}{\partial t} \right) = \frac{\partial}{\partial z} \left( \kappa_i \frac{\partial T_i}{\partial z} \right), i = 2 \text{ or } 3 \quad (3)$$

$$-\kappa_1 \frac{\partial T_1}{\partial z} \Big|_{z=\text{interface}} = -\kappa_2 \frac{\partial T_2}{\partial z} \Big|_{z=\text{interface}} = G(T_1 - T_2) \Big|_{z=\text{interface}} \quad (4)$$

Where  $\rho$  is the density,  $c$  is the specific heat in  $\text{Jkg}^{-1}\text{K}^{-1}$ ,  $\kappa$  is the thermal conductivity,  $T$  is the temperature, and  $Source$  is the source term due to pump laser heating. Note that the final volumetric heat capacity extracted from the model is  $c_v = \rho c \text{Jm}^{-3}\text{K}^{-1}$ .  $R_{pump}$  is the reflectivity of the absorption layer at the pump laser wavelength,  $F$  is the laser fluence,  $t_p$  is the pulse width,  $\delta$  is the optical

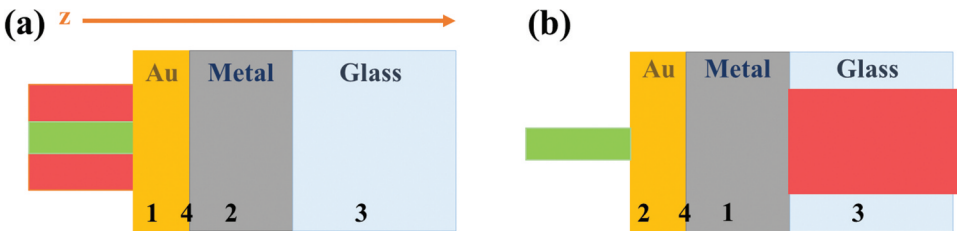


**Figure 2.** Schematics for the sample configuration and the pump-and-probe geometry for the ps-TTR system (a) and ps-LF system (b). For the ps-TTR measurement, layer 1 indicates the layer that absorbs the energy of the pump laser and also reflects the CW probe laser. Its temperature profile is described in Equation (1) with the source term described in Equation (2). For the ps-LF measurement, the pump energy is absorbed in the metal film near the metal/glass interface. In both cases, layer 2 and 3 are the layers that do not absorb the pump, described with Equation (3). 4 is the interface expressed in Equation (4).

absorption depth, and  $L$  is the thickness of the absorbing layer.  $G$  is the interfacial thermal conductance between layers. This model simulates heat dissipation in both ps-TTR and ps-LF setups. Note that the only difference between them is the source term's position due to setup variations. In ps-TTR, the gold transducer absorbs all pump laser energy due to gold's optical penetration depth of 12.2 nm for 1064 nm laser, far shorter than the gold layer thickness. Consequently, the source term *Source* is only nonzero within the gold layer. Conversely, with ps-LF, the pump penetrates the glass substrate and is directly absorbed near the metal/glass interface. The optical penetration depths of the 1064 nm laser within measured metals are below 23.7 nm, significantly less than the metal layer thickness (297 nm to 1.2  $\mu\text{m}$ ), making the source term nonzero exclusively within the metal layer. In both scenarios, the time-dependent normalized temperature change is extracted from the top of the gold layer.

With two data sets and two simulated curves, we conduct a global fitting with shared parameters using the least squares method. In Figure 3, A flowchart is used to describe the global fitting process. Due to the Au/Metal/Glass structure of our samples, the fitting parameters are the heat capacity and thermal conductivity of the metal film ( $c_{v,metal}$  and  $\kappa_{metal}$ ) as well as the interfacial thermal resistance between the Au and the metal layers ( $R_{Au/metal} = 1/G_{Au/metal}$ ). The input parameters fixed during the fitting process are  $c_{v,Au}$ ,  $\kappa_{Au}$ ,  $c_{v,Glass}$ ,  $\kappa_{Glass}$ ,  $d_{Au}$ ,  $d_{metal}$ ,  $d_{Glass}$  and  $R_{metal/Glass}$  [32, 33]. At the beginning of the fitting, we give initial guess values of the fitting parameters [ $c_{v,metal}$ ,  $\kappa_{metal}$ ,  $R_{Au/metal}$ ]. Using those values, we simulate normalized temperature change at the gold surface using the 1D heat dissipation model for both ps-TTR and ps-LF. The sum of squared residuals (s.s.r.) is computed by summing the squared differences between experimental data and simulated curves at each time point, divided by the total number of points. The goal is to minimize the summed s.s.r. for ps-TTR and ps-LF by varying the values of [ $c_{v,metal}$ ,  $\kappa_{metal}$ ,  $R_{Au/metal}$ ]. We use the MATLAB function *fminsearch* for iterative optimization. In each iteration, the [ $c_{v,metal}$ ,  $\kappa_{metal}$ ,  $R_{Au/metal}$ ] changes based on the Nelder-Mead method [34], and the summation of the s.s. r. for ps-TTR and ps-LF is calculated. The iterations end when the difference in summation between iterations drops below the tolerance level, yielding the fitting results for parameters [ $c_{v,metal}$ ,  $\kappa_{metal}$ ,  $R_{Au/metal}$ ].

Plotted in Figure 4a, b are the normalized fitting curves compared with the normalized experimental data measured in titanium thin film. With ps-TTR, the criteria for choosing the fitting time range are described in previous paper, that the time range should maximize the area underneath the sensitivity curve (Figure 5a, c) [20]. Meanwhile, the fitting time should not be too long where the reflectivity change signal is small, thus the low signal-to-noise ratio would induce extra uncertainty in

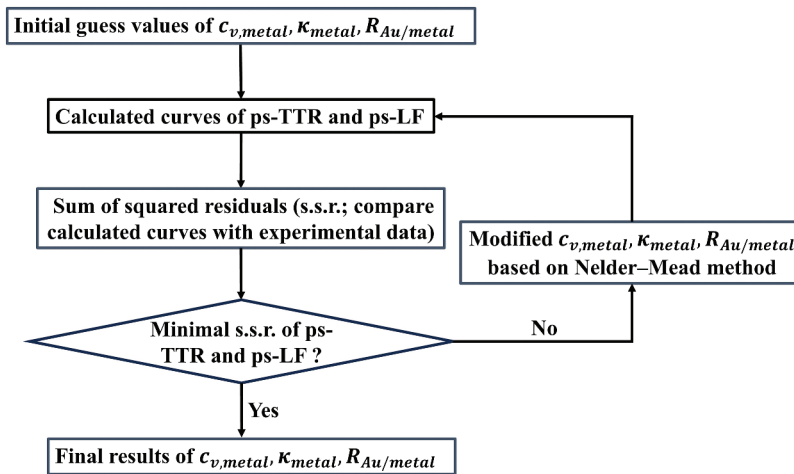
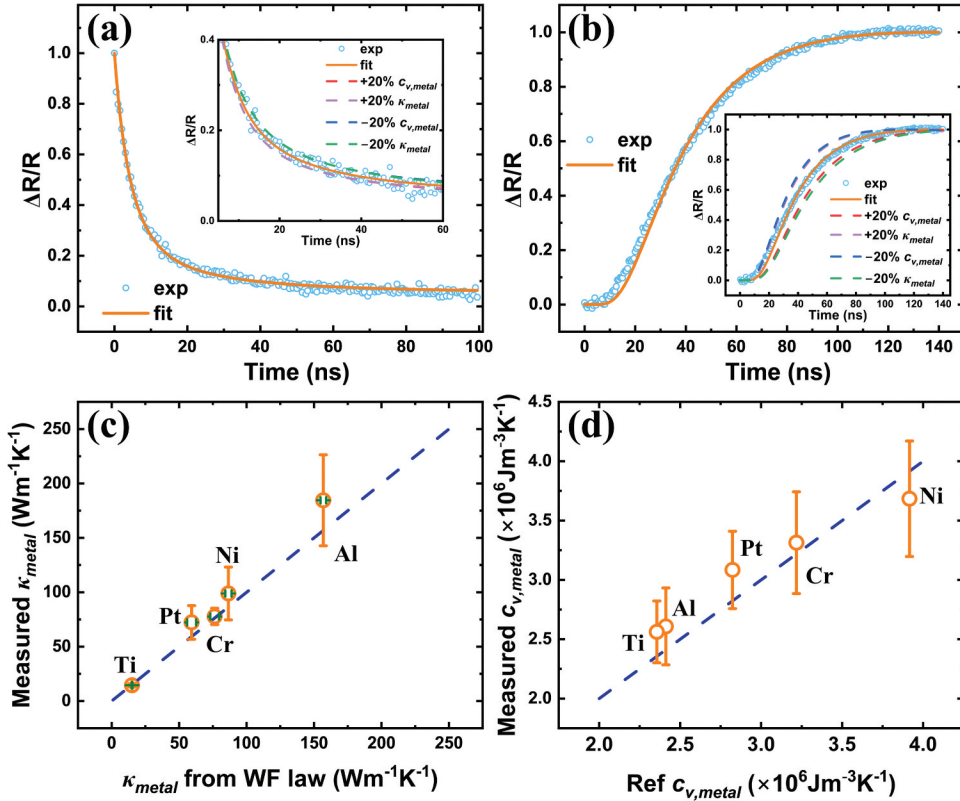


Figure 3. Illustration of global fitting process with experimental results from both ps-TTR and ps-LF. "s.s.r." denotes the sum of squared residuals.





**Figure 4.** Normalized experimental reflectivity change of probe and simulation curves with best-fitted  $\kappa_{metal}$  and  $c_{v,metal}$  from (a) ps-TTR and (b) ps-LF measurements of titanium film. The insets are the simulation curves with a 20% variation of the  $\kappa_{metal}$  or  $c_{v,metal}$ . The best-fitted thermal conductivity (c) and heat capacity (d) are compared with the reference values [32, 35].

the final fitting result. For all the ps-TTR experiments, we choose the first 100 ns as the fitting time range. With ps-LF, the fitting is most sensitive to the temperature-rising part (Figure 5b, d), so we choose the signal range where the temperature starts to rise until the temperature reaches its maximum. Along with the experimental data and the best-fitted curves, we plot the confidence intervals by varying the best-fitted  $c_{v,metal}$  and  $\kappa_{metal}$  values by  $\pm 20\%$ . For ps-TTR (Figure 4a, inset), the  $+20\% \kappa_{metal}$  and  $+20\% c_{v,metal}$  almost overlap with each other, which is consistent with the fact that ps-TTR results are sensitive to the effusivity, the multiplication of  $\kappa_{metal}$  and  $c_{v,metal}$ . For ps-LF (Figure 4b, inset), the  $+20\% c_{v,metal}$  shows a similar trend with  $-20\% \kappa_{metal}$ , indicating that ps-LF results are sensitive to diffusivity. The best-fitted  $\kappa_{metal}$  and  $c_{v,metal}$  values for all five samples with their uncertainties (Refer to section S2 in the supplementary material for uncertainty evaluation) are plotted in Figure 4c, d against reference values. Reference thermal conductivity is determined using the four-point probe method (Cascade Summit 11,000 AP and Keithley 4200-SCS), measuring sheet resistance, and converting it to thermal conductivity with the Wiedemann-Franz law. Heat capacity employs literature data [32, 35]. All the measured values with our ps-TTR + ps-LF approach agree well with reference values, affirming its reliability for simultaneous determination of  $\kappa_{metal}$  and  $c_{v,metal}$ .

Next, we'll consider the sensitivity of this combined approach. The sensitivity (S) of the model is calculated by evaluating the change in the temperature curve (T) with respect to the change of independent parameters ( $x_0$ ):  $S = \frac{\partial \ln T}{\partial \ln x_0}$  [36]. According to the Au/Metal/Glass structure of our samples, as shown in Figure 2, the multi-layer model contains three layers, and the independent

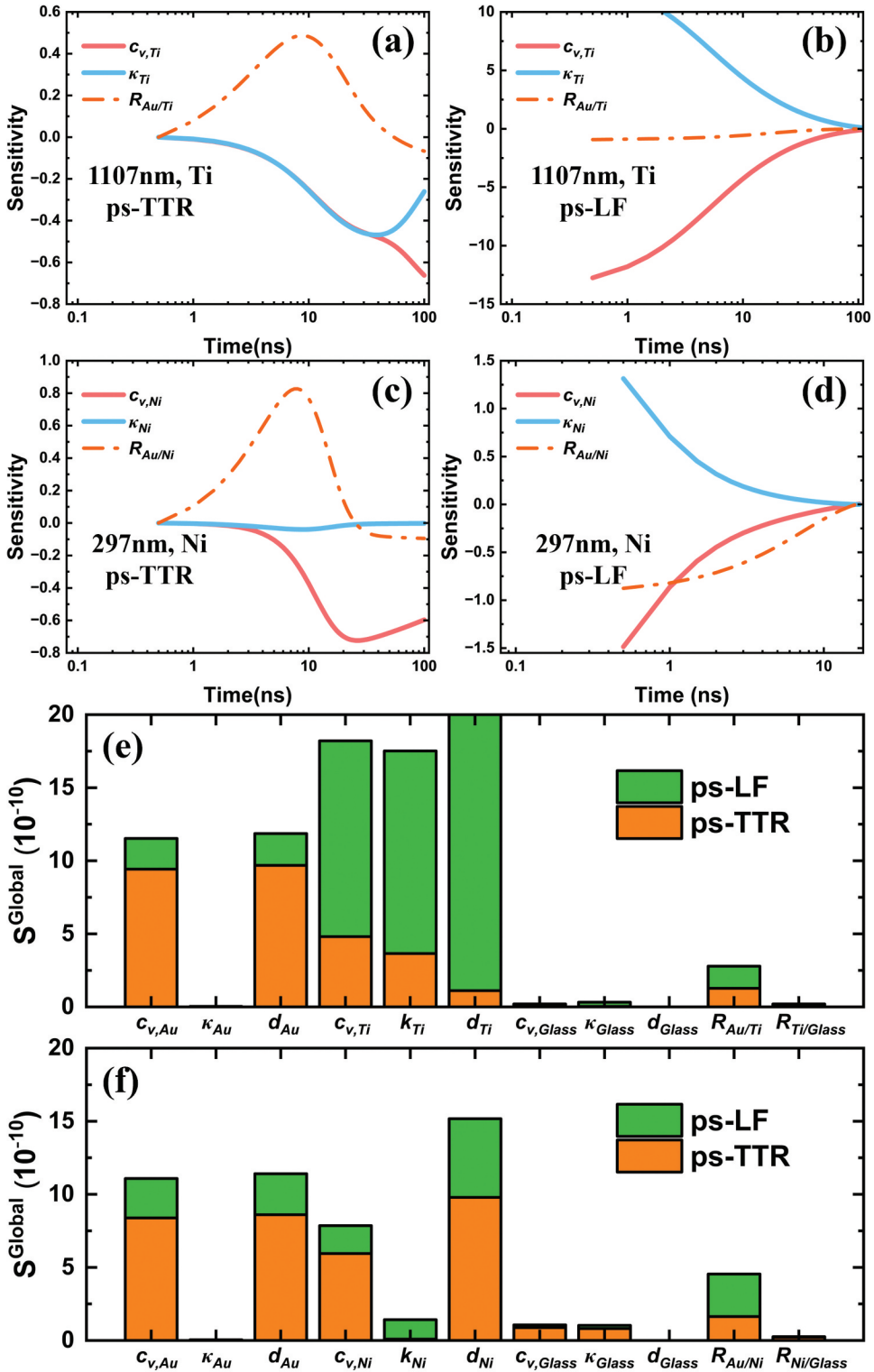


**Figure 5.** Representative sensitivity tests for the 1.1  $\mu$ m-thick titanium film using ps-TTR (a) and ps-LF (b) and for 297 nm-thick nickel film using ps-TTR (c) and ps-LF (d). And the improved sensitivity with global fitting compared with individual ps-LF or ps-TTR for cases of Ti (e) and Ni films (f).



variables are the thickness ( $d$ ), thermal conductivity ( $\kappa$ ), volumetric heat capacity ( $c_v$ ) of all three layers, as well as the interface thermal resistance between them ( $R$ ).

We start with the sensitivity test of the ps-TTR and the ps-LF separately. Figure 5a, b show an example of a sensitivity test on titanium film with 1.1  $\mu\text{m}$  thickness (For the sensitivity test of all parameters, please see Figure. S7 in the supplementary material). In Figure 5a, the sensitivities of the volumetric heat capacity and the thermal conductivity of the titanium film are both negative in the ps-TTR configuration and follow the same trend until the sensitivity of the thermal conductivity ( $\kappa_{Ti}$ ) starts to decrease, at which point the heat passes through the metal layer and reaches the glass substrate. This tendency indicates that when heat travels within the titanium layer, the thermal response is governed by effusivity  $\varepsilon$ . Higher heat capacity and larger thermal conductivity of the titanium film would increase the rate of heat dissipation in the gold layer and bring down the surface temperature quicker. Therefore, the sensitivities are negative. For the case of ps-LF (Figure 5b), the sensitivities of heat capacity and thermal conductivity have opposite trends because the higher  $\kappa$  leads to faster temperature rising on the probe side, while larger heat capacity causes more heat storage in the titanium layer and slows down the heat propagation. So the thermal response for the ps-LF case is governed by the thermal diffusivity  $\alpha$ . Figure 5c, d show the sensitivity of the 297 nm-thick Ni film on the glass substrate, the thinnest sample tested. The  $\kappa_{Ni}$  is unlikely to be determined with ps-TTR alone due to the fact that the sensitivity is less than 0.1. However, considering the large sensitivity of  $\kappa_{Ni}$  and  $c_{v,Ni}$  in ps-LF, the  $\kappa_{Ni}$  can be extracted with low uncertainty in the combined method, which will be discussed below. One thing worth pointing out is that the sensitivities (for the interfacial thermal resistance between Ti/Glass and Ni/Glass (Refer to Fig. S7 in the supplementary material for sensitivity of interfacial thermal resistance)) are negligible for both configurations. Thus, we didn't set the interfacial thermal conductance between metal and glass as a fitting parameter. Instead, we set the interfacial thermal conductance as a constant:  $G_{metal/Glass} = 50\text{MWm}^{-2}\text{K}^{-1}$ , which is around the average value of the metal/Glass interfacial thermal conductance we measured previously in the ps-TTR experiments [20] and also similar with the interfacial thermal conductance between gold and metal layers ( $G_{Au/metal}$ ) that we measured in the current experiment (Fig. S8 in the supplementary material).

Secondly, we want to discuss the benefit of our combined method on sensitivity. Since we use the global fitting to fit the experimental curves of both ps-TTR and ps-LF simultaneously, when considering the sensitivity, we should not focus on one of the cases only. The low sensitivity in ps-TTR (ps-LF) can be compensated by the high sensitivity in ps-LF (ps-TTR). For better clarification, we calculate the integrated sensitivity parameters with normalization [19]:

$$S_{x_0}^{\text{Global}} = \left( \frac{\int_0^{t_f} S_{x_0} dt}{t_f} \right)_{\text{ps-TTR}} + \left( \frac{\int_0^{t_f} S_{x_0} dt}{t_f} \right)_{\text{ps-LF}} \quad (5)$$

Where  $x_0$  represent all the parameters, including the input and fitting parameters.  $S_{x_0}$  is the sensitivity of that parameter, which is a function of time.  $t_f$  is the total fitting time. In Figure 5e, f, we plot the  $S_{x_0}^{\text{Global}}$  to show the compensation effect. For example, the thermal conductivity of nickel film is insensitive to ps-TTR, while the extra sensitivity is contributed by ps-LF. Please note that Equation (5) is not an accurate description of the actual sensitivity from global fitting since the fitting minimizes the summation of s.s.r.s from ps-TTR and ps-LF, not individually, while the orange and green blocks in Figure 5e, f are calculated from solely ps-TTR or ps-LF.

This compensation effect yields reduced uncertainty of the  $\kappa$  and  $c_v$ . Figure 4c, d plot the measured  $\kappa$  and  $c_v$  values along with uncertainties, which are all below 25% and 15%, respectively. The uncertainties are mainly propagated from input parameter uncertainties and experimental signal noise. To compare with ps-TTR, we calculate titanium film's thermal conductivity uncertainty for both ps-TTR alone and the combined method. When solely using ps-TTR experimental data, the

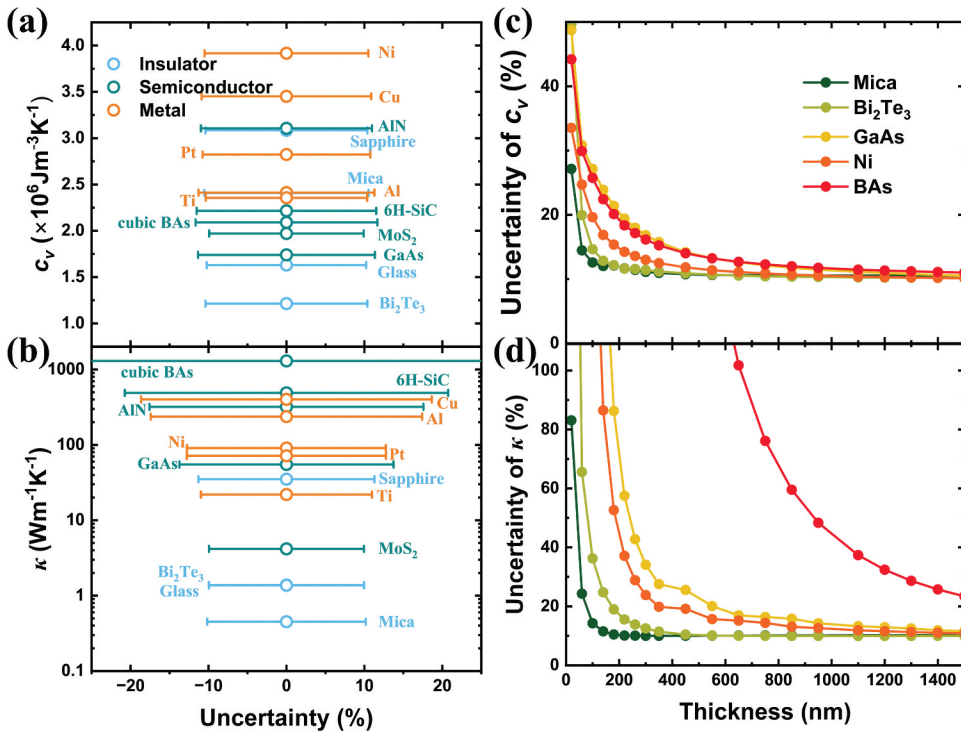


**Figure 6.** Uncertainty analysis on several representative materials [32,35,37–51]. (a) Materials with different  $c_v$  and their uncertainties. (b) Materials with different  $\kappa$  and their uncertainties. (c) Thickness dependent uncertainties of  $c_v$  for selected materials. (d) Thickness dependent uncertainties of  $\kappa$ .

thermal conductivity uncertainty is 24.9% [20]. With this combined approach, the thermal conductivity uncertainty is reduced to 10.3%.

To assess the applicability of our combined method across various materials, we proceed to calculate the corresponding uncertainties for different materials when measured using this approach. Since not all the materials are opaque and have short absorption depth, another gold layer is inserted between the material and the glass substrate as the absorption layer in ps-LF configurations. We use the 50 nm-Au/Material/50 nm-Au/Glass structure in all the simulations and calculate the uncertainties. Figure 6a, b shows the uncertainties of 1  $\mu\text{m}$ -thick material with different heat capacities and thermal conductivities. The uncertainties of the heat capacity are all below 25% and vary within a small range for most materials. There is no obvious relationship between uncertainties and the actual  $c_v$  values. The uncertainty of  $\kappa$ , on the other hand, is higher for larger  $\kappa$ , due to the faster heat penetration through the thin film and less effective time range. To determine the minimum thickness that can be possibly measured, we also calculate the uncertainties at different thicknesses (Figure 6c, d). We define the minimum thickness that our combined setup can measure as those at which both uncertainties of  $c_v$  and  $\kappa$  are below 25%. Overall, the uncertainties of the  $c_v$  drop below 25% at 140 nm for all selected materials with wide  $c_v$  and  $\kappa$  range (Figure 6c). It is the uncertainty of  $\kappa$  that determines the minimum thickness. For materials with low thermal conductivity, such as mica, the minimum thickness can be as small as 60 nm. For ultrahigh thermal conductivity material, such as cubic BAS, the minimum thickness is about 1400 nm. The minimum thickness could be further pushed to smaller values if the time resolution of data measurement can be improved. Currently, the resolution of our photo-detector is 500 ps. With a faster detector, more data points could be acquired that give better performance during the fitting process, especially when the sample is thin. For very thick samples,

high laser fluence is required, especially for the ps-LF measurement, so that the temperature rise on the probe side is high enough to give a good signal-to-noise ratio. When laser fluence is too high, the Au transducer film could be damaged, which poses another restriction of this method, similar to traditional laser flash.

There are also other techniques to measure the thermal conductivity of thin films, such as the most common  $3\omega$  and TDTR (time domain thermoreflectance). The minimum thickness that  $3\omega$  can measure is limited by the thermal conductivity ratio between the film and the substrate, and the width of the metal line, so it would be hard to measure the thermal conductivity of submicron-thick thin film [36]. For TDTR, the minimum thickness that can be measured is governed by the smallest penetration depth. Accurate measurement of the thin film's thermal conductivity requires high sensitivity to the  $\kappa_{film}$  while low sensitivity to the substrate thermal conductivity, which means that the thermal penetration depth should be controlled as less than half of the thin film thickness. The thermal penetration depth  $d_{th}$  is reversely correlated to the modulation frequency  $f$  as  $d_{th} = \sqrt{\frac{\alpha}{\pi f}}$ , where  $\alpha$  is the diffusivity of the film [52]. With the conventional TDTR, the maximum modulation frequency is usually 20 MHz, beyond which the low output signal leads to large noise. Thus, the minimum thermal penetration depth is limited. Taking the Nickel case for comparison, the penetration depth of Ni at 20 MHz is 653 nm using the measured thermal conductivity and heat capacity. Jiang et al. extended the limitation of thin film measurement with TDTR by measuring two sets of data at different modulation frequencies and taking the signal ratio of these two measurements as the final signal for fitting [28]. This approach can improve the sensitivity of  $\kappa_{film}$  by suppressing the sensitivities of other parameters that are always large in the high frequency range, such as the thickness of the transducer layer. The minimum thickness that this method can measure is  $0.85d_{th}$ , but the sensitivity of the thin film heat capacity is sacrificed. For Ni, this dual-frequency method can extend the minimum thickness to 555 nm. With our combined approach, the Ni film measured has a thickness of 297 nm Ni and both the thermal conductivity and heat capacity values are consistent to the reference values. Our combined technique offers unique advantages on measuring thermal properties with high accuracy. Another way is to treat the thin layer as the interface, but it requires the knowledge of the interfacial resistances between the thin film and adjacent layers (metal transducer and substrate) to extract the thermal conductivity, making the process even more complicated.

The combined approach described in this report offers unique advantages in characterizing thermal conductivity and heat capacity with low uncertainties, which have many potential applications in different research fields. Our experimental setup is compatible with most optically transparent chambers, including cryostat and diamond anvil cell (DAC), to enable in-situ thermal characterization at extreme conditions where phase transition happens. Previous research has shown the complexity of the heat capacity and the thermal diffusivity near phase transition [53, 54], which leads to the difficulties in determining thermal conductivity [53]. Our combined setup can extract the total  $c_v$  and  $k$  altogether, providing the true thermal conductivity value, and separating the contributions from lattice evolution and phase transition, although further careful examination is still required.

Recently, phase change materials (PCMs) have been utilized in chip thermal management due to the high latent heat that absorbs the heat and reduces the chip's peak temperature. Among various PCM options, the solid-solid phase transition materials offer lower volume change and are container-free, leading to a more compact circuit design [55]. The thermal conductivities of PCMs range from 0.2 W/mK to 70 W/mK, while the heat capacities are between  $0.7 \times 10^6$  J/m<sup>3</sup>K and  $2.4 \times 10^6$  J/m<sup>3</sup>K, both are within the measurable range of our combined technique [56].

In summary, we developed a combined approach with the ps-TTR and ps-LF methods for simultaneous determination of the heat capacity and thermal conductivity. Five metal films with thicknesses ranging from 297 nm to 1.2  $\mu$ m were tested, and the obtained values for thermal conductivity and heat capacity are consistent with reference data, with uncertainties below 25% and 15%, respectively. The low uncertainty mainly results from the fact that the sensitivities of

the ps-TTR and ps-LF can compensate for each other. Considering the short optical absorption depth and zero band gap of the metal we use in this study, no extra layer of gold between the metal layer and glass layer is required for heat generation. While for the thermal properties measurement on other materials with either long optical absorption depth or band gap larger than the pump laser wavelength, an extra layer of gold is needed to absorb the pump laser. Potential applications of the new methodology in thermal management, phase transitions in solid-state physics, and planetary sciences in extreme pressures and temperatures are discussed to highlight the potential impacts of the study.

## Acknowledgments

The authors are grateful for the support from National Science Foundation (CBET-2211660). The authors thank Dr. Xiaojia Wang (Department of Mechanical Engineering, University of Minnesota) for her invaluable inputs and suggestions to this work.

## Disclosure statement

No potential conflict of interest was reported by the author(s).

## Funding

This work was supported by National Science Foundation (CBET-2211660).

## ORCID

Janghan Park  <http://orcid.org/0000-0002-3735-3657>  
Yanyao Zhang  <http://orcid.org/0000-0002-3846-1131>  
Matthew Disiena  <http://orcid.org/0009-0004-0335-1276>  
Sanjay K. Banerjee  <http://orcid.org/0000-0002-4478-7189>  
Jung-Fu Lin  <http://orcid.org/0000-0002-0163-5329>  
Yaguo Wang  <http://orcid.org/0000-0002-0448-5645>

## References

- [1] F. Guillou, *et al.* “Non-hysteretic first-order phase transition with large latent heat and giant low-field magnetocaloric effect.” *Nat. Commun.*, vol. 9, no. 1, 2018. DOI: [10.1038/s41467-018-05268-4](https://doi.org/10.1038/s41467-018-05268-4).
- [2] R. H. Busey, and W. F. Giauque, “The Heat Capacity of Mercury from 15 to 330° K. Thermodynamic Properties of Solid Liquid and Gas. Heat of Fusion and Vaporization1.” *J. Am. Chem. Soc.*, vol. 75, no. 4, pp. 806–809, 1953.
- [3] V. K. Pecharsky, K. A. Gschneidner, and D. Fort, “Superheating and other unusual observations regarding the first order phase transition in Dy.” *Scr. Mater.*, vol. 35, no. 7, pp. 843–848, 1996. DOI: [10.1016/1359-6462\(96\)00225-4](https://doi.org/10.1016/1359-6462(96)00225-4).
- [4] M. M. H. Polash, M. Rasoulianboroujeni, and D. Vashae, “Magnon and spin transition contribution in heat capacity of ferromagnetic Cr-doped MnTe: Experimental evidence for a paramagnetic spin-caloritronic effect.” *Appl. Phys. Lett.*, vol. 117, no. 4, 2020. DOI: [10.1063/5.0011887](https://doi.org/10.1063/5.0011887).
- [5] A. Szewczyk, M. Gutowska, and B. Dabrowski, “Specific heat and phase diagram of heavily doped La<sub>1-x</sub>Sr<sub>x</sub>MnO<sub>3</sub> (0.45 ≤ x ≤ 1.0).” *Phys. Rev. B - Condens. Matter Mater. Phys.*, vol. 72, no. 22, pp. 1–8, 2005. DOI: [10.1103/PhysRevB.72.224429](https://doi.org/10.1103/PhysRevB.72.224429).
- [6] N. T. H. Kim-Ngan, *et al.*, “Superconductivity in the splat-cooled UMo alloys,” *Adv. Nat. Sci.: Nanosci. Nanotechnol.*, vol. 6, no. 1, pp. 015007, 2015. DOI: [10.1088/2043-6262/6/1/015007](https://doi.org/10.1088/2043-6262/6/1/015007).
- [7] J. Kačmarčík *et al.* “Specific heat of superconducting MgCNi<sub>3</sub> single crystals.” *J. Phys. Conf. Ser.*, vol. 150, no. 5, pp. 3–7, 2009. DOI: [10.1088/1742-6596/150/5/052087](https://doi.org/10.1088/1742-6596/150/5/052087).
- [8] D. G. Cahill, “Analysis of heat flow in layered structures for time-domain thermoreflectance,” *Rev. Sci. Instrum.*, vol. 75, no. 12, pp. 5119–5122, Dec. 2004. DOI: [10.1063/1.1819431](https://doi.org/10.1063/1.1819431).
- [9] W. J. Parker, R. J. Jenkins, C. P. Butler, and G. L. Abbott, “Flash method of determining thermal diffusivity, heat capacity, and thermal conductivity.” *J. Appl. Phys.*, vol. 32, no. 9, pp. 1679–1684, 1961. DOI: [10.1063/1.1728417](https://doi.org/10.1063/1.1728417).

- [10] T. Baba and A. Ono, "Improvement of the laser flash method to reduce uncertainty in thermal diffusivity measurements." *Meas. Sci. Technol.*, vol. 12, no. 12, pp. 2046, 2001. DOI: [10.1088/0957-0233/12/12/304](https://doi.org/10.1088/0957-0233/12/12/304).
- [11] N. Taketoshi, T. Baba, and A. Ono, "Observation of heat diffusion across submicrometer metal thin films using a picosecond thermoreflectance technique." *Jpn. J. Appl. Phys.*, vol. 38, no. 11A, pp. L1268, 1999. DOI: [10.1143/JJAP.38.L1268](https://doi.org/10.1143/JJAP.38.L1268).
- [12] N. Taketoshi, T. Baba, and A. Ono, "Development of a thermal diffusivity measurement system for metal thin films using a picosecond thermoreflectance technique." *Meas. Sci. Technol.*, vol. 12, no. 12, pp. 2064, 2001. DOI: [10.1088/0957-0233/12/12/306](https://doi.org/10.1088/0957-0233/12/12/306).
- [13] N. Taketoshi, T. Baba, and A. Ono, "Electrical delay technique in the picosecond thermoreflectance method for thermophysical property measurements of thin films." *Rev. Sci. Instrum.*, vol. 76, no. 9, Sep 2005. DOI: [10.1063/1.2038628](https://doi.org/10.1063/1.2038628).
- [14] T. Baba, N. Taketoshi, and T. Yagi, "Development of ultrafast laser flash methods for measuring thermophysical properties of thin films and boundary thermal resistances." *Jpn. J. Appl. Phys.*, vol. 50, no. 11, pp. 11RA01, Nov 2011. PART 2. DOI: [10.1143/JJAP.50.11RA01](https://doi.org/10.1143/JJAP.50.11RA01).
- [15] T. Yagi, *et al.*, "Analysis on thermal properties of tin doped indium oxide films by picosecond thermoreflectance measurement," *J. Vac. Sci. Technol. A Vacuum, Surfaces, Film*, vol. 23, no. 4, pp.1180–1186, 2005. DOI: [10.1116/1.1872014](https://doi.org/10.1116/1.1872014).
- [16] T. Baba, "Analysis of one-dimensional heat diffusion after light pulse heating by the response function method." *Jpn. J. Appl. Phys.*, vol. 48, no. 5, pp. 05EB04, May. 2009. DOI: [10.1143/JJAP.48.05EB04](https://doi.org/10.1143/JJAP.48.05EB04).
- [17] L. Chen, A. M. Limarga, and D. R. Clarke, "A new data reduction method for pulse diffusivity measurements on coated samples," *Comput. Mater. Sci.*, vol. 50, no. 1, pp. 77–82, Nov. 2010. DOI: [10.1016/j.commatsci.2010.07.009](https://doi.org/10.1016/j.commatsci.2010.07.009).
- [18] K. Hatori, N. Taketoshi, T. Baba, and H. Ohta, "Thermoreflectance technique to measure thermal effusivity distribution with high spatial resolution." *Rev. Sci. Instrum.*, vol. 76, no. 11, pp. 1–7, 2005. DOI: [10.1063/1.2130333](https://doi.org/10.1063/1.2130333).
- [19] R. Garrelts, A. Marconnet, and X. Xu, "Assessment of thermal properties via nanosecond thermoreflectance method," *Nanoscale Microscale Thermophys. Eng.*, vol. 19, no. 4, pp.245–257, 2015. DOI: [10.1080/15567265.2015.1078425](https://doi.org/10.1080/15567265.2015.1078425).
- [20] J. Jeong, *et al.* "Picosecond transient thermoreflectance for thermal conductivity characterization." *Nanoscale Microscale Thermophys. Eng.*, vol. 23, no. 3, 211–221, Jul. 2019. DOI: [10.1080/15567265.2019.1580807](https://doi.org/10.1080/15567265.2019.1580807).
- [21] A. J. Schmidt, X. Chen, and G. Chen, "Pulse accumulation, radial heat conduction, and anisotropic thermal conductivity in pump-probe transient thermoreflectance." *Rev. Sci. Instrum.*, vol. 79, no. 11, 2008. DOI: [10.1063/1.3006335](https://doi.org/10.1063/1.3006335)
- [22] A. J. Schmidt, R. Cheaito, and M. Chiesa, "A frequency-domain thermoreflectance method for the characterization of thermal properties." *Rev. Sci. Instrum.*, vol. 80, no. 9, 2009. DOI: [10.1063/1.3212673](https://doi.org/10.1063/1.3212673)
- [23] J. Yang, C. Maragliano, and A. J. Schmidt, "Thermal property microscopy with frequency domain thermoreflectance." *Rev. Sci. Instrum.*, vol. 84, no. 10, 2013. DOI: [10.1063/1.4824143](https://doi.org/10.1063/1.4824143)
- [24] J. Liu, *et al.*, "Simultaneous measurement of thermal conductivity and heat capacity of bulk and thin film materials using frequency-dependent transient thermoreflectance method." *Rev. Sci. Instrum.*, vol. 84, no. 3, Mar. 2013. DOI: [10.1063/1.4797479](https://doi.org/10.1063/1.4797479)
- [25] X. Wang, C. D. Liman, N. D. Treat, M. L. Chabinyk, and D. G. Cahill, "Ultralow thermal conductivity of fullerene derivatives." *Phys. Rev. B - Condens. Matter Mater. Phys.*, vol. 88, no. 7, pp. 1–7, 2013. DOI: [10.1103/PhysRevB.88.075310](https://doi.org/10.1103/PhysRevB.88.075310).
- [26] J. B. Henderson, J. A. Wiebelt, and M. R. Tant, "A method for the determination of the specific heat and heat of decomposition of composite materials," *Thermochim. Acta*, vol. 57, no. 2, pp.161–171, 1982. DOI: [10.1016/0040-6031\(82\)80057-9](https://doi.org/10.1016/0040-6031(82)80057-9).
- [27] M. J. O'Neill, "Measurement of specific heat functions by differential scanning calorimetry." *Anal. Chem.*, vol. 38, no. 10, pp. 1331–1336, 1966. DOI: [10.1021/ac60242a011](https://doi.org/10.1021/ac60242a011).
- [28] P. Jiang, B. Huang, and Y. K. Koh, "Accurate measurements of cross-plane thermal conductivity of thin films by dual-frequency time-domain thermoreflectance (TDTR)." *Rev. Sci. Instrum.*, vol. 87, no. 7, 2016. DOI: [10.1063/1.4954969](https://doi.org/10.1063/1.4954969)
- [29] R. B. Wilson, B. A. Apgar, L. W. Martin, and D. G. Cahill, "Thermoreflectance of metal transducers for optical pump-probe studies of thermal properties." *Opt. Express*, vol. 20, no. 27, pp. 28829, 2012. DOI: [10.1364/oe.20.028829](https://doi.org/10.1364/oe.20.028829).
- [30] I. H. Chowdhury and X. Xu, "Heat transfer in femtosecond laser processing of metal," *Numer. Heat Transf. Part A Appl.*, vol. 44, no. 3, pp.219–232, 2003. DOI: [10.1080/716100504](https://doi.org/10.1080/716100504).
- [31] L. Guo, S. L. Hodson, T. S. Fisher, and X. Xu, "Heat transfer across metal-dielectric interfaces during ultrafast-laser heating." *J Heat Transfer*, vol. 134, no. 4, pp. 1–5, 2012. DOI: [10.1115/1.4005255](https://doi.org/10.1115/1.4005255).
- [32] Y. S. Touloukian and E. H. Bucoy, *Thermophysical Properties of Matter - The TPRC Data Series. Volume 4. Specific Heat - Metallic Elements and Alloys*, vol. 4, no. Specific Heat. 1971.
- [33] Y. S. Touloukian, R. K. Kirby, R. E. Taylor, and P. D. Desai, *Thermophysical Properties of Matter - The TPRC Data Series. Volume 1. Thermal Conductivity - Metallic Elements and Alloys*. 1970.
- [34] J. C. Lagarias, J. A. Reeds, M. H. Wright, and P. E. Wright, "Convergence properties of the Nelder–Mead simplex method in low dimensions," *SIAM J. Optim.*, vol. 9, no. 1, pp.112–147, 1998. DOI: [10.1137/S1052623496303470](https://doi.org/10.1137/S1052623496303470).
- [35] C. Y. Ho, R. W. Powell, and P. E. Liley, "Thermal conductivity of the elements: A comprehensive review." *J. Phys. Chem. Ref. Data*, vol. 3, 1974. DOI: [10.1063/1.3253100](https://doi.org/10.1063/1.3253100).



- [36] Y. K. Koh, *et al.* "Comparison of the  $3\omega$  method and time-domain thermoreflectance for measurements of the cross-plane thermal conductivity of epitaxial semiconductors." *J. Appl. Phys.*, vol. 105, no. 5, 2009. DOI: [10.1063/1.3078808](https://doi.org/10.1063/1.3078808).
- [37] J. S. Kang, M. Li, H. Wu, H. Nguyen, and Y. Hu, "Experimental observation of high thermal conductivity in boron arsenide," *Science (80-)*, vol. 361, no. 6402, pp.575–578, 2018. DOI: [10.1126/science.aat5522](https://doi.org/10.1126/science.aat5522).
- [38] N. P. Gorbachuk and V. R. Sidorko, "Heat capacity and enthalpy of Bi<sub>2</sub>Si<sub>3</sub> and Bi<sub>2</sub>Te<sub>3</sub> in the temperature range 58–1012 K," *Poroshkovaya Metall.*, vol. 43, no. 5–6, pp.79–86, 2004. DOI: [10.1023/B:PMMC.0000042464.28118.a3](https://doi.org/10.1023/B:PMMC.0000042464.28118.a3).
- [39] I. T. Witting, *et al.* "The thermoelectric properties of bismuth telluride." *Adv. Electron. Mater.*, vol. 5, no. 6, pp. 1–20, 2019. DOI: [10.1002/aelm.201800904](https://doi.org/10.1002/aelm.201800904).
- [40] J. S. Blakemore, "Semiconducting and other major properties of gallium arsenide." *J. Appl. Phys.*, vol. 53, no. 10, 1982. DOI: [10.1063/1.331665](https://doi.org/10.1063/1.331665).
- [41] H. J. Goldsmid and A. E. Bowley, "Thermal conduction in mica along the planes of cleavage," *Nature*, vol. 187, no. 4740, pp.864–865, 1960. DOI: [10.1038/187864a0](https://doi.org/10.1038/187864a0).
- [42] A. S. Gray and C. Uher, "Thermal conductivity of mica at low temperatures." *J. Mater. Sci.*, vol. 12, no. 5, pp. 959–965, 1977. DOI: [10.1007/BF00540978](https://doi.org/10.1007/BF00540978).
- [43] A. Bano, P. Khare, and N. K. Gaur, "Thermal transport properties of bulk and monolayer MoS<sub>2</sub>: An ab-initio approach," *J. Phys. Conf. Ser.*, vol. 836, no. 1, pp.012052, 2017. DOI: [10.1088/1742-6596/836/1/012052](https://doi.org/10.1088/1742-6596/836/1/012052).
- [44] V. Varshney, *et al.*, "MD simulations of molybdenum disulphide (MoS<sub>2</sub>): Force-field parameterization and thermal transport behavior." *Comput. Mater. Sci.*, vol. 48, no. 1, pp. 101–108, 2010. DOI: [10.1016/j.commatsci.2009.12.009](https://doi.org/10.1016/j.commatsci.2009.12.009).
- [45] D. A. Ditmars, S. Ishihara, S. S. Chang, G. Bernstein, and E. D. West, "ENTHALPY and HEAT-CAPACITY STANDARD REFERENCE MATERIAL: SYNTHETIC SAPPHIRE (alpha -Al<sub>2</sub>O<sub>3</sub>) from 10 to 2250 K." *J. Res. Natl. Bur. Stand. (United States)*, vol. 87, no. 2, pp. 159–163, 1982. DOI: [10.6028/jres.087.012](https://doi.org/10.6028/jres.087.012).
- [46] P. Jiang, X. Qian, X. Gu, and R. Yang, "Probing anisotropic thermal conductivity of transition metal dichalcogenides MX<sub>2</sub> (M = Mo, W and X = S, Se) using time-domain thermoreflectance," *Adv. Mater. Weinheim*, vol. 29, no. 36, pp.1–7, 2017. DOI: [10.1002/adma.201701068](https://doi.org/10.1002/adma.201701068).
- [47] F. Medjdoub and K. Iniewski. "Gallium Nitride (GaN)." *Gallium Nitride (GaN)*, 2017. DOI: [10.4324/b19387](https://doi.org/10.4324/b19387).
- [48] B. Salce, *et al.*, "Thermal conductivity of pure and Si-doped CuGeO<sub>3</sub>," *Phys. Lett. Sect. A Gen. At. Solid State Phys.*, vol. 245, no. 1–2, pp.127–132, 1998. DOI: [10.1016/S0375-9601\(98\)00347-8](https://doi.org/10.1016/S0375-9601(98)00347-8).
- [49] L. Boteler, A. Lelis, M. Berman, and M. Fish, "Thermal conductivity of power semiconductors-when does it matter?," *2019 IEEE 7th Work. Wide Bandgap Power Devices Appl. WiPDA 2019*, pp. 265–271, 2019, DOI: [10.1109/WiPDA46397.2019.8998802](https://doi.org/10.1109/WiPDA46397.2019.8998802).
- [50] F. James, E. J. F. Shackelford, and W. Alexander, *CRC materials science and engineering handbook*, CRC press, 2000. DOI: [10.1201/9781420038408](https://doi.org/10.1201/9781420038408).
- [51] J. Yang, E. Ziade, and A. J. Schmidt, "Uncertainty analysis of thermoreflectance measurements." *Rev. Sci. Instrum.*, vol. 87, no. 1, 2016. DOI: [10.1063/1.4939671](https://doi.org/10.1063/1.4939671)
- [52] P. Jiang, X. Qian, and R. Yang, "A new elliptical-beam method based on time-domain thermoreflectance (TDTR) to measure the in-plane anisotropic thermal conductivity and its comparison with the beam-offset method." *Rev. Sci. Instrum.*, vol. 89, no. 9, 2018. DOI: [10.1063/1.5029971](https://doi.org/10.1063/1.5029971)
- [53] H. Chen, *et al.*, "Thermal conductivity during phase transitions." *Adv. Mater. Weinheim.*, vol. 31, no. 6, pp. 1–7, 2019. DOI: [10.1002/adma.201806518](https://doi.org/10.1002/adma.201806518).
- [54] M. T. Agne, P. W. Voorhees, and G. J. Snyder, "Phase transformation contributions to heat capacity and impact on thermal diffusivity, thermal conductivity, and thermoelectric performance." *Adv. Mater. Weinheim.*, vol. 31, no. 35, pp. 1–7, 2019. DOI: [10.1002/adma.201902980](https://doi.org/10.1002/adma.201902980).
- [55] C. R. Raj, S. Suresh, R. R. Bhavsar, and V. K. Singh, "Recent developments in thermo-physical property enhancement and applications of solid solid phase change materials: A review." *J. Therm. Anal. Calorim.*, vol. 139, no. 5, pp. 3023–3049, 2020. DOI: [10.1007/s10973-019-08703-w](https://doi.org/10.1007/s10973-019-08703-w).
- [56] W. Hua, L. Zhang, and X. Zhang. "Research on passive cooling of electronic chips based on PCM: A review." *J. Mol. Liq.*, vol. 340, pp. 117183, 2021. DOI: [10.1016/j.molliq.2021.117183](https://doi.org/10.1016/j.molliq.2021.117183).